PAPER IN FOREFRONT

**Frank Ottinger · Ivana Kroslakova ·
Kathrin Hametner · Eric Reusser · Reinhard Nesper ·
Detlef Günther**

Analytical evidence of amorphous microdomains within nitridosilicate and nitridoaluminosilicate single crystals

Abstract Single crystals of new nitridosilicates and nitrido-aluminosilicates with excellent R values in X-ray investigations were analysed quantitatively using 30 to 60 μm single-spot LA-ICP-MS. Significant discrepancies between expected and measured chemical composition could not be explained by the crystallographic data. High spatial resolution analysis using electron probe microanalysis (EPMA, 10 μm) leads to the discovery of inhomogeneities in the crystalline material. The application of standard single-spot LA-ICP-MS with a spatial resolution of 30 to 60 μm is not suitable for the analysis of these crystals as the existing inhomogeneities dominate and alter the determined concentrations. However, owing to the better detection capabilities, a scanning LA-ICP-MS procedure enables a more representative analysis of single crystals of $Ca_5Si_2Al_2N_8$ than single-spot LA-ICP-MS as a result of a larger sampling volume. It is highly likely that these impurities consist of amorphous, vitreous phases as powder diffraction X-ray data indicates the existence of a significant fraction of an X-ray amorphous material besides crystalline silicates. These microdomains contain less aluminium, silicon and calcium or are nearly free of aluminium, which explains the detected discrepancies in the chemical composition.

Keywords Nitridosilicates · Single crystals · Microprobe · LA-ICP-MS

F. Ottinger · I. Kroslakova · K. Hametner ·
R. Nesper · D. Günther (✉)
ETH Zurich, Laboratory of Inorganic Chemistry,
8093 Zurich, Switzerland
e-mail: guenther@inorg.chem.ethz.ch

E. Reusser
ETH Zurich, Institute for Mineralogy and Petrology,
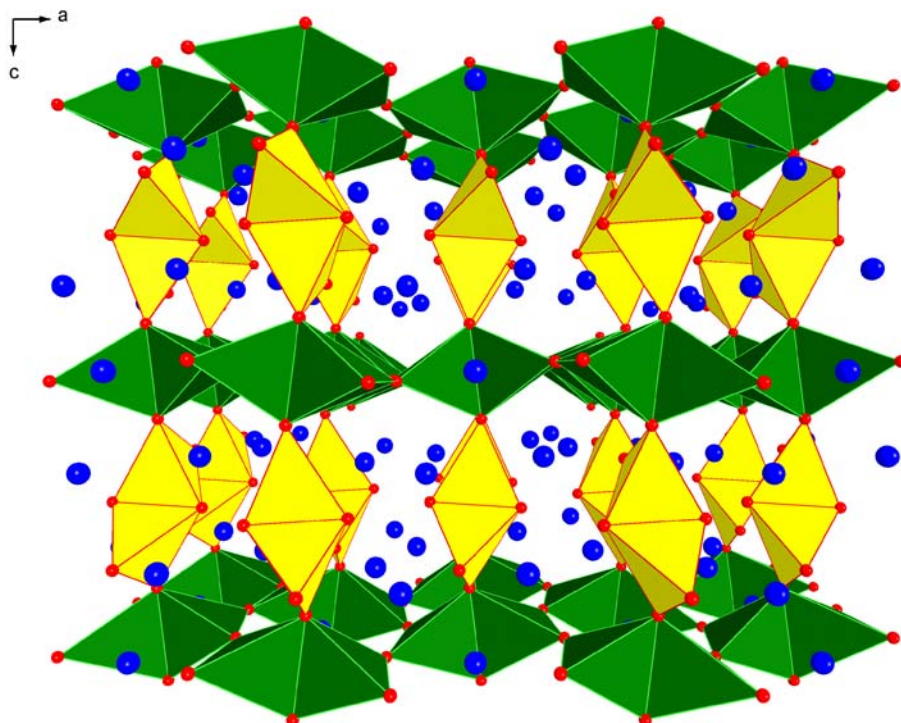8092 Zurich, Switzerland

Introduction

Oxosilicates are the largest known class of minerals combining two of the most abundant elements in the earth's crust. A very large number of oxosilicate phases with an enormous diversity of structures have been investigated, whereas nitrogen-containing silicates are relatively unexplored [1–9]. Nitridosilicates can be derived from oxosilicates by a formal exchange of oxygen with nitrogen, i.e. they contain SiN_4 instead of SiO_4 tetrahedra. Consequently, the high possible degree of crosslinking in nitridosilicates leads predominantly to three-dimensional network structures. The compounds exhibit outstanding chemical and physical stability and are of interest for this reason.

Among the wide variety of direct solid analysis techniques available, laser ablation inductively coupled plasma mass spectrometry (LA-ICP-MS) has become one of the major analytical methods to determine elemental concentrations within solids [10–12]. The high sensitivity of this technique allows the direct determination of major, minor and trace elements within a spatial resolution of few tens of micrometres. Therefore, the major application of this technique is geology, where in situ trace element analysis within different mineral phases can be assessed [13]. Furthermore, a variety of powder and sediment samples have been analysed to gain information about the trace element distribution, which can be used for studies into the climate and environmental pollution [14, 15]. However, recent studies in material science indicate a growing interest in applying this technique for trace element determinations in high-purity materials such as CaF_2 [16], the trace element determination in zeolites [17] and furthermore measurements of element concentrations in Si-B-C-N high-durable ceramic materials [18]. It has been shown that the detection capabilities of the technique are sufficient to measure the trace element impurities in concentrations as low as few ng g^{-1}. The major element concentration ratios were determined with a precision of approximately 2–5%.

Fig. 1 Anionic network structure of $Ca_5Si_2Al_2N_8$. Closed AlN_4 tetrahedra (*dark green*), SiN_4 tetrahedra (*yellow*), Ca^{2+} cations (*blue balls*). View along [010]

Fundamental studies in LA-ICP-MS have shown that the sampling process, the aerosol transport and the excitation of the generated aerosols are still not fully understood [19], such that each new application requires a thorough validation of the analytical data. Since the materials of interest within this study are synthetic samples and no external reference materials for the quantification are available, a detailed analytical study on a variety of inorganic materials was carried out and the data were used to describe new synthesised nitridosilicates and nitridoaluminosilicates.

The aim of this study was to determine the stoichiometric composition of nitridosilicates and possible synthesis-derived impurities by using LA-ICP-MS. Since impurities are expected in the $\mu g\ g^{-1}$ concentration range this technique is most sensitive for multielement analysis of solids. Therefore, a variety of samples were analysed using spatially resolved analysis. The NIST 610 glass reference material was used for external calibration and Ca was used as internal standard. Since no matrix-matched calibration material was available for this study, mineral samples (Wollastonite and Grossular) with closely related composition were also analysed. To verify the data acquired by LA-ICP-MS, electron probe microanalysis (EPMA) was also applied to selected samples for validation purposes.

Fig. 2 Anionic network structure of $Ca_4SiAl_3N_7$. Closed AlN_4 tetrahedra (*dark green*), mixed $SiAlN_4$ tetrahedra (*light green*), SiN_4 tetrahedra (*yellow*), Ca^{2+} cations (*blue balls*). View along [100]
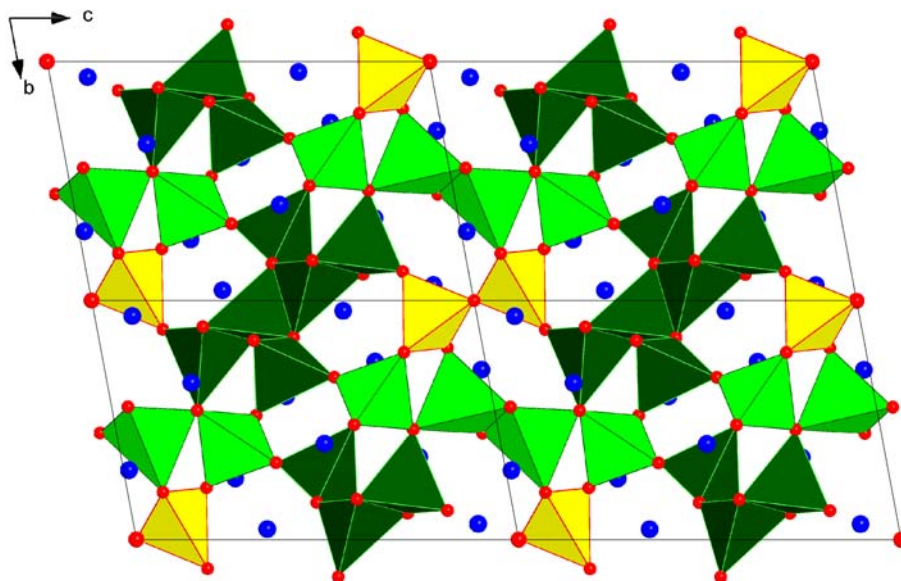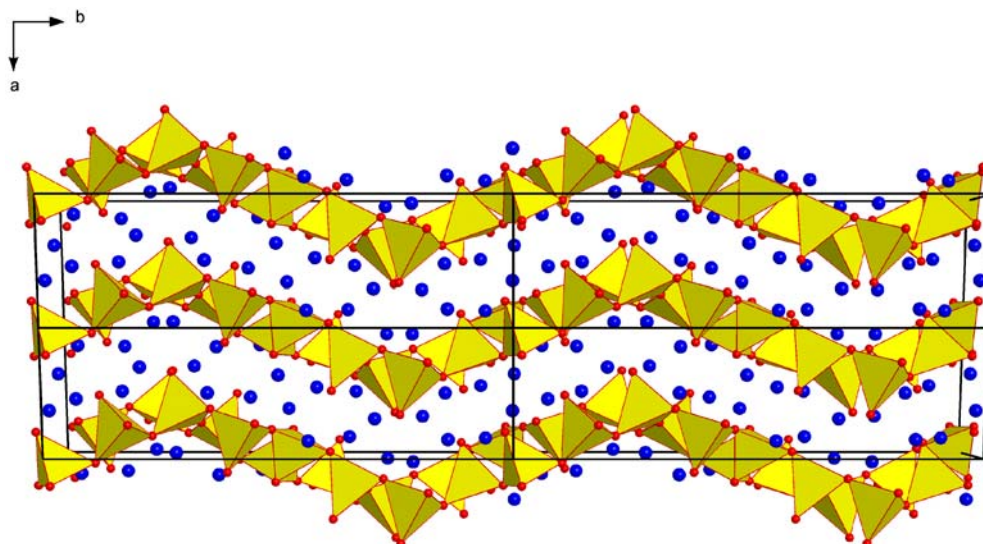
Fig. 3 Anionic layer structure of $Ca_7Si_4N_{10}$. Closed SiN_4 tetrahedra (yellow), Ca^{2+} cations (blue balls). View along [001]

Experimental

The synthesis and characterisation of nitridoaluminosilicates or nitridosilicates with a low degree of condensation is challenging due to their reactivity and high affinity for hydrolysis or oxidation in air. In contrast, nitridosilicates with a high degree of condensation exhibit an extraordinary stability towards concentrated mineral acids or bases [9]. We were able to open up a new synthetic pathway to the first nitridoaluminosilicates $Ca_5Si_2Al_2N_8$ and $Ca_4SiAl_3N_7$ as well as the nitridosilicate $Ca_7Si_4N_{10}$ by reaction of binary calcium nitrides or subnitrides with silicon and/or aluminium in closed niobium or tantalum ampoules at

Table 1 Operating conditions for laser sampling and ICP-MS measurements

Parameter	Value
Laser type	ArF excimer
Laser wavelength	193 nm
Spot diameter (sample and standard)	30–60 µm
Repetition rate sample	5 Hz
Repetition rate standard	10 Hz
Laser energy	170 mJ
He carrier gas flow rate	1 L min^{-1}
RF Power	1,410 W
Nebulizer gas flow rate	0.7 L min^{-1}
Auxiliary gas flow rate	0.85 L min^{-1}
Coolant gas flow rate	16 L min^{-1}
Lens settings	Autolens
Number of sweeps	2
Number of readings	320
Number of replicates	1
Dwell time	10 ms
Detector mode	Dual (pulse and analog)
Number of measured elements	11
Ablation duration	1 min

temperatures well above 1,200°C [20]. These nitridoaluminosilicates are the first structurally identified compounds of the last missing member in the $A_mT_nX_p$ family of silicates (A=cations; T=Si and/or Al; X=O and/or N).

All of the abovementioned new compounds exhibit a so far unknown structure type. $Ca_5Si_2Al_2N_8$ and $Ca_4SiAl_3N_7$ crystallise with three-dimensional network structures (Fig. 1 and 2) and can therefore be classified as tectosilicates, whereas $Ca_7Si_4N_{10}$ with its puckered layered structure (Fig. 3) can be identified as a phyllosilicate. Although $Ca_5Si_2Al_2N_8$ and $Ca_4SiAl_3N_7$ possess a high degree of condensation (0.5 and 0.57), both compounds are not stable to diluted mineral acids in contrast to nitridosilicates with a similar degree of condensation. Not surprisingly, $Ca_7Si_4N_{10}$ decomposes when exposed to water due to its layered structure and its low degree of condensation.

The crystallographic investigation of single crystals of all three compounds leads to unambiguous structural solutions. They can all be refined down to very small R values ($Ca_7Si_4N_{10}$ 2.65%, $Ca_5Si_2Al_2N_8$ 1.61%, $Ca_4SiAl_3N_7$ 3.27%) leaving no space for structural speculations. We have found no crystallographic indication for mixed or not fully occupied atomic sites or for atoms heavier than Ca.

Since Si^{4+} and Al^{3+} or O^{2-} and N^{3-} have similar atomic form factors, a clear differentiation between these ions is very difficult and sometimes impossible based on X-ray data only. The allocation in Si^{4+} and Al^{3+} succeeds for $Ca_5Si_2Al_2N_8$ on the basis of Si–N and Al–N bond distances, with Al–N bonds being significantly longer than Si–N bonds. Such a differentiation does not succeed for $Ca_4SiAl_3N_7$ relying on X-ray diffraction experiments only. The computation of Madelung factors, lattice energies and point potentials permits the generation of a plausible Si/Al distribution for this compound [20].

Based on that data alone, one cannot exclude possible phase ranges for these compounds according to $Ca_7Si_{4-x}Al_xN_{10-x}O_x$, $Ca_5Si_{2-x}Al_{2+x}N_{8-x}O_x$ and $Ca_4Si_{1-x}Al_{3+x}N_{7-x}O_x$, demonstrating their close relationship to sialons.

Table 2 Variation of the mass distribution in $Ca_5Si_{2-x}Al_{2+x}O_xN_{8-x}$ with $0 \leq x \leq 0.6$

x	Formula	M (g mol⁻¹)	wt%				
			Ca	Si	Al	O	N
0	$Ca_5Si_2Al_2N_8$	422.58	47.42	13.30	12.77	0	26.52
0.1	$Ca_5Si_{1.9}Al_{2.1}O_{0.1}N_{7.9}$	422.67	47.41	12.63	13.41	0.38	26.18
0.2	$Ca_5Si_{1.8}Al_{2.2}O_{0.2}N_{7.8}$	422.76	47.40	11.96	14.04	0.76	25.84
0.3	$Ca_5Si_{1.7}Al_{2.3}O_{0.3}N_{7.7}$	422.84	47.39	11.29	14.68	1.14	25.51
0.4	$Ca_5Si_{1.6}Al_{2.4}O_{0.4}N_{7.6}$	422.93	47.38	10.63	15.31	1.51	25.17
0.5	$Ca_5Si_{1.5}Al_{2.5}O_{0.5}N_{7.5}$	423.02	47.37	9.96	15.95	1.89	24.83
0.6	$Ca_5Si_{1.4}Al_{2.6}O_{0.6}N_{7.4}$	423.11	47.36	9.20	16.58	2.27	24.50

Laser ablation sampling was performed using an ArF 193 nm excimer laser (GeoLas Q, MicroLas, Göttingen, Germany) which was coupled to an ICP-MS instrument (Elan 6100 DRC+Perkin Elmer, SCIEX, Concord, Ontario, Canada). The operating conditions of the instrumentation are summarised in Table 1.

The samples were ablated in single crater mode at a spatial resolution of 60 μm and a repetition rate of 5 and 10 Hz. Within an analysis sequence of 20 analyses, each individual analysis consisted of 30 s gas blank measurements followed by 60 s ablation of the sample. Standards were measured twice at the beginning of a run and twice at the end of the analyses. The quantification procedure was based on external calibration using NIST (National Institute for Standards and Technology), SRM 610 and internal standardization. The use of an internal standard allows correction for differences in the mass ablated between the sample of interest and reference material, differences in the transport behaviour of the laser generated aerosols and also as drift correction for processes within the plasma [21]. For analysis of solids in their natural state, a naturally occurring internal standard (e.g. calcium is very often the element of choice owing to its abundance in many minerals) is recommended for quantification [22]. The concentration of the element which is supposed to be used as internal standard must therefore be known prior to the analysis and should be homogeneously distributed within the sample of interest. We obtained the concentration of the internal standard element by calculating its concentration

from the stoichiometry of the mineral or using an alternative method (in our case EPMA) to determine its concentration in the sample. Due to the atmospheric nature of the ICP, oxygen and nitrogen cannot be measured using this technique.

Calcium was chosen as an internal standard as a result of its crystallographic unambiguousness. Substitution of Al with Si and N with O for $Ca_5Si_2Al_2N_8$ could lead to a possible phase width $Ca_5Si_{2-x}Al_{2+x}O_xN_{8-x}$ with $0 \leq x \leq 2$. The analyses revealed that this range shows an upper limit of x=0.6. Nevertheless, calcium is the most suitable internal standard owing to the negligible change in overall mass shown in Table 2. Even at x=0.6 the mass fraction of Ca declines marginally from 47.42 wt% to 47.36 wt%. The implemented uncertainty by the standardization is significantly below the precision of the method and can therefore be neglected for this investigated phase. The same argumentation is valid for $Ca_7Si_{4-x}Al_xN_{10-x}O_x$ and $Ca_4Si_{1-x}Al_{3+x}N_{7-x}O_x$.

Before analysing the synthetic samples, the quantification procedure was tested using minerals. To investigate the ablation behaviour of Ca in relation to Al and Si, Grossular and Wollastonite minerals with closely matched compositions were analyzed within this study. These studies were of importance since matrix effects in the ICP may occur, which are also called "elemental fractionation effects" [23–26].

Quantification of Grossular was based on Ca as internal standard. The Ca concentration was calculated from the

Table 3 Results of LA-ICP-MS analysis of Grossular using Ca as internal standard

Measurement	Measured concentrations (wt%)					
	⁴²Ca: Theoretical			⁴²Ca: EPMA		
	²⁷Al	²⁹Si	⁴²Ca	²⁷Al	²⁹Si	⁴²Ca
1	8.77	19.57	26.69	8.66	19.33	26.76
2	8.95	19.15	26.69	8.85	18.92	26.76
3	8.96	19.24	26.69	8.85	19.01	26.76
4	8.68	19.54	26.69	8.58	19.30	26.76
5	8.61	19.38	26.69	8.51	19.15	26.76
Summary						
Average (wt%)	8.8	19.4	26.7	8.7	19.1	26.8
Standard deviation (wt%)	0.16	0.18	–	0.16	0.18	–
RSD (%)	1.79	0.95	–	1.84	0.93	–
Recovery (%)	73.4	103.7	–	86.1	105.3	–

Ca concentration applied for quantification was based on stoichiometry and concentrations determined by EPMA

Table 4 Results of the LA-ICP-MS analysis of Wollastonite minerals using Ca (34.50 wt% based on theoretical values) as internal standard

Measurement	Measured concentrations (wt%)			
	^{42}Ca	Quebec ^{29}Si	Bazene ^{29}Si	Oravitza ^{29}Si
1	34.50	25.01	23.75	23.42
2	34.50	24.07	24.54	24.12
3	34.50	24.17	24.12	22.76
4	34.50	24.31	24.31	23.23
5	34.50	24.07	24.12	23.18
Summary				
Average (wt%)	34.5	24.3	24.2	23.3
Standard deviation (wt%)	–	0.39	0.29	0.50
RSD (%)	–	1.60	1.20	2.14
Recovery (%)	–	100.6	100.0	96.5

ditions for quantitative analysis and image acquisition were an acceleration voltage of 15 kV, a beam current of 15 nA and a beam diameter <100 nm. The X-ray lines selected for analysis were $Ca - K_\alpha$ at a wavelength of 0.33595 nm, $Al - K_\alpha$ at 0.83401 nm and $Si - K_\alpha$ at 0.71262 nm. The monochromator crystals used were PET for Ca and TAP for Al and Si.

The standards used were pure $CaCO_3$ (calcite) crystals for calcium, pure Al_2O_3 (corundum) for aluminium and pure SiO_2 (quartz) for silicon. The sample was coated with a 20-nm layer of carbon. All measurements were corrected for detector dead time, instrumental drift and X-ray background. For the correction of the inter-element effects (i.e. absorption, fluorescence) the CITZAF code was applied [27]. Nitrogen was not measured directly because of the strong absorption of its X-ray radiation by the matrix leading to big uncertainties. Therefore, nitrogen was calculated by difference to 100%.

stoichiometry (Ca=26.69 wt%) and the concentration determined by EPMA measurement (Ca=26.37 wt%, see Table 3). The theoretical composition of Grossular, $Ca_3Al_2Si_3O_{12}$, was calculated from its stoichiometry: Ca=26.69 wt%, Al=11.98 wt%, Si=18.70 wt%. The experimental element distribution of that mineral determined from EPMA measurements shows a different composition: Ca=26.76±0.08 wt%, Al=10.25±0.26 wt%, Si=18.45±0.15 wt%.

For further evaluation of the accuracy of the Ca/Si concentration ratios, another naturally occurring mineral Wollastonite ($CaSiO_3$) was analysed. The theoretical composition of Wollastonite was calculated from its stoichiometry: Ca=34.50 wt%, Si=24.18 wt%. Three Wollastonite minerals, Quebec, Bazene and Oravitza, obtained from different regions were analysed with the corresponding concentration ratios summarized in Table 4. The recovery of the Si concentration based on internal standardization using Ca within natural minerals indicates the suitability of LA-ICP-MS for these types of samples. Therefore, it can be concluded that the analysis of nitrogen-containing silicate samples using the same analytical procedure should lead to similar results.

The electron probe microanalysis (EPMA) was performed on a JEOL JXA 8200 instrument equipped with a 5-wavelength dispersive X-ray spectrometer (WDS) and an energy dispersive spectrometer (EDS). Electron beam con-

Results and discussion

Since the early application of laser ablation, Ca has always been the preferred internal standard for trace element determinations [22]. However, ablation studies using a 266-nm laser ablation system revealed that Ca/Si ratios can vary significantly [24]. More recent investigations on the influence of the wavelength on the ablation behaviour of various matrices have shown that the shorter wavelength leads to significantly reduced fractionation effects [28–30]. Furthermore, recent studies on the stoichiometric composition of laser-generated aerosols also indicated that the stoichiometric composition of the material entering the excitation source represents the original sample [31]. Therefore it can be concluded that any deviation of the ICP-MS signal intensities measured must be influenced by different ionization of particles of the reference material (NIST 610) and the sample within the ICP. However, since it is also known that 193 nm produces the smallest particle fractions (ca. below 200 nm), these effects should be significantly reduced [25]. The results on natural minerals summarised in Table 3 acquired using 193 nm demonstrate that the achievable precision and accuracy for these types of samples and deviations as obtained in ref. [24] were not observed. Therefore, LA-ICP-MS analyses on a single

Table 5 Results of the LA-ICP-MS analyses of a single crystal of $Ca_5Si_2Al_2N_8$ using Ca (47.42 wt% based on theoretical values) as internal and NIST 610 as external standard, all concentrations in $\mu g\ g^{-1}$

Isotope	^{7}Li	^{23}Na	^{25}Mg	^{27}Al	^{28}Si	^{29}Si	^{30}Si	^{35}Cl	^{42}Ca	^{43}Ca	^{44}Ca	^{57}Fe	^{88}Sr	^{93}Nb	^{153}Eu
Replicate 1	46	88	10	136,800	96,800	98,000	99,100	29	474,200	456,100	403,900	123	45	101	1
Replicate 2	26	106	7	133,400	98,600	98,400	98,900	57	474,200	461,300	459,300	135	46	85	1
Replicate 3	115	506	10	134,800	95,000	93,600	93,000	47	474,200	452,100	413,200	113	41	47	1
Replicate 4	4	1	8	137,900	100,700	99,600	100,600	45	474,200	491,000	470,000	100	44	44	1
Replicate 5	14	36	7	134,300	103,800	102,200	99,500	50	474,200	461,100	468,100	123	45	91	1
Average	41	147	8	135,400	99,000	98,400	98,300	46	474,200	464,300	442,900	119	44	74	1
Standard deviation	44	204	1	1,800	3,400	3,100	2,900	10		15,400	31,800	14	2	26	0

Table 6 Results of the LA-ICP-MS analyses of a single crystal of $Ca_4SiAl_3N_7$ using Ca (43.63 wt% based on theoretical values) as internal and NIST 610 as external standard, all concentrations in $\mu g\ g^{-1}$

Isotope	^7Li	^{23}Na	^{27}Al	^{28}Si	^{29}Si	^{30}Si	^{35}Cl	^{42}Ca	^{43}Ca	^{44}Ca	^{57}Fe	^{88}Sr	^{90}Zr	^{93}Nb	^{153}Eu	^{181}Ta
Replicate 1	1	2	231,400	48,100	42,000	39,900	42	436,300	429,600	377,900	100	25	1	11,000	1	8
Replicate 2	36	1	231,700	46,600	45,200	42,500	43	436,300	449,100	437,800	97	24	1	11,400	1	7
Replicate 3	4	27	220,400	41,900	39,000	37,700	51	436,300	417,100	374,300	103	24	2	22,700	1	17
Replicate 4	3	2	214,400	43,700	39,100	38,700	52	436,300	421,500	372,700	105	25	1	23,100	1	17
Replicate 5	59	13	212,300	47,000	44,500	42,900	50	436,300	423,100	375,900	104	24	1	11,700	1	9
Average	21	9	222,000	45,400	42,000	40,400	48	436,300	428,092	387,700	102	24	1	13,000	1	12
Standard deviation	26	11	9,200	2,600	2,900	2,300	5		12,600	28,000	3	1	0	6,300	0	5

Table 7 Results of the LA-ICP-MS analyses of a single crystal of $Ca_7Si_4N_{10}$ using Ca (52.64 wt% based on theoretical values) as internal and NIST 610 as external standard, all concentrations in $\mu g\ g^{-1}$

Isotope	^7Li	^{23}Na	^{25}Mg	^{27}Al	^{29}Si	^{30}Si	^{35}Cl	^{42}Ca	^{43}Ca	^{44}Ca	^{57}Fe	^{88}Sr	^{93}Nb
Replicate 1	1	1	134	31,500	136,300	129,800	236	526,400	494,200	482,200	25	109	125
Replicate 2	1	1	165	26,200	162,000	15,020	220	526,400	514,300	490,500	24	110	284
Replicate 3	5	2	162	20,900	137,200	130,000	206	526,400	488,500	487,400	53	107	265
Replicate 4	1	1	147	29,200	151,600	145,000	335	526,400	527,700	484,300	14	123	245
Replicate 5	1	1	151	23,700	150,300	142,300	188	526,400	517,500	491,400	21	118	261
Average	2	1	152	26,300	147,500	139,500	237	526,400	508,400	487,100	27	113	236
Standard deviation	2	1	13	4,200	10,800	9,100	58		16,400	3,900	15	7	64

crystal of $Ca_5Si_2Al_2N_8$ were carried out to investigate the Al/Si concentration ratio as well as the concentration and distribution of trace element impurities. The concentrations of the single-spot analyses are summarised in Table 5.

Five replicate single-spot analyses were carried out on the same single crystal. Quantification was based on NIST 610 and internal standardization using Ca (^{42}Ca using the nominal concentration of 47.42 wt% in $Ca_5Si_2Al_2N_8$). The isotopes ^7Li, ^{11}B, ^{23}Na, $^{25,26}Mg$, ^{27}Al, $^{28,29,30}Si$, $^{35,37}Cl$, ^{39}K, $^{42-44}Ca$, ^{53}Cr, ^{55}Mn, $^{54,56,57}Fe$, ^{72}Ge, ^{88}Sr, ^{90}Zr, ^{93}Nb,

Table 8 Results of the LA-ICP-MS analyses of twelve single crystals of $Ca_5Si_2Al_2N_8$ using NIST 610 and BCR 2G as an external standard and calcium as an internal standard

	Al	Si	Σ Al+Si	Absolute difference
Crystal 1	13.54	9.89	23.43	2.63
Crystal 2	11.58	10.73	22.31	3.75
Crystal 3	11.16	10.00	21.16	4.90
Crystal 4	12.08	9.65	21.73	4.33
Crystal 5	12.29	10.85	23.14	2.92
Crystal 6	12.34	10.72	23.06	3.00
Crystal 7	11.59	10.24	21.83	4.23
Crystal 8	12.14	10.30	22.44	3.62
Crystal 9	12.05	10.57	22.62	3.44
Crystal 10	12.61	10.60	23.21	2.85
Crystal 11	10.82	10.51	21.33	4.73
Crystal 12	11.48	9.66	21.14	4.92
Average	11.97	10.31	22.28	3.78
Standard deviation	0.72	0.42	1.14	1.14

All concentrations are given in wt%. The last column shows the absolute difference to the expected sum value of 26.06 wt%

^{153}Eu, ^{178}Hf and ^{181}Ta with limits of detection of $1-10\ ng\ g^{-1}$ were measured. Only the elements given in the table were significantly above the limits of detection. The ubiquitous occurrence of sodium was detected at an average concentration of 147 $\mu g\ g^{-1}$. However, the precision indicates a highly variable distribution of this element within the synthesized crystal. Li, Mg, Cl, Fe, Sr, Nb and Eu are trace elements present in the single crystal with a maximum concentration of 100 $\mu g\ g^{-1}$ ($1-119\ \mu g\ g^{-1}$). These results indicate that this single crystal consists mainly of calcium, silicon and aluminium without further significant impurities (Table 6).

However, the determined concentrations of Al and Si were determined to be significantly different from their theoretical concentration. The sum of both elements was theoretically expected to be 26.06 wt% instead of the detected 23.43 wt%. The absolute difference of 2.63 wt% from the expected value or the relative deviation of 11.2% was also not explainable by a contribution of other elements present in the matrix. The individual concentration of Al at 13.54±0.18 wt% was significantly higher than its expected value of 12.77 wt%. In contrast, the concentration of Si at 9.89±0.34 wt% was determined to be significantly below the theoretical value of 13.29 wt%.

To elucidate the influence of interferences, three different isotopes were measured for Ca and Si. Excluding the contribution of mass bias, no significant influences due to interferences were obtained. Therefore, possible contributions of $^{14}N^{14}N^{14}N$, $^{28}Si^{14}N$, $^{29}Si^{14}N$ or $^{28}Si^{16}O$ clusters on the isotopes ^{42}Ca, ^{43}Ca or ^{44}Ca can be excluded to be responsible for the underestimation of Si and slight overestimation of Al. However, in the case of an interference on the internal standard, both elements would be influenced in
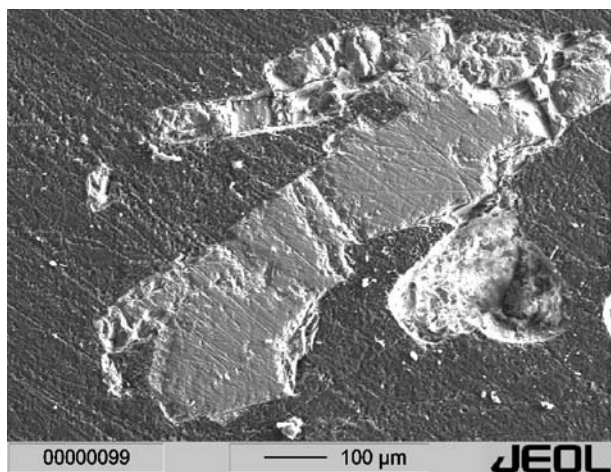
Fig. 4 Electron microscope picture using secondary electrons of single crystals of $Ca_5Si_2Al_2N_8$ embedded in methacrylate resin

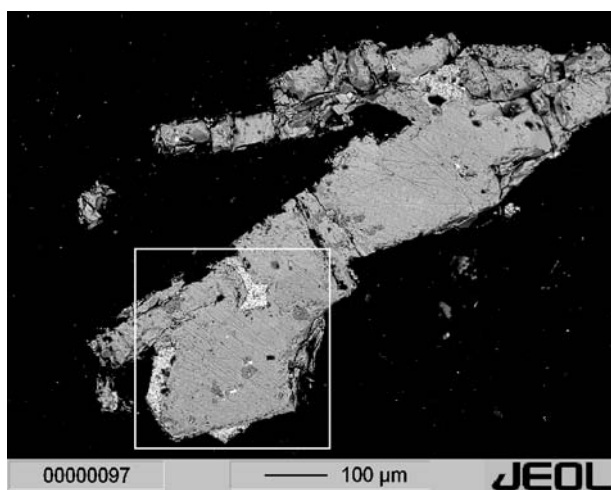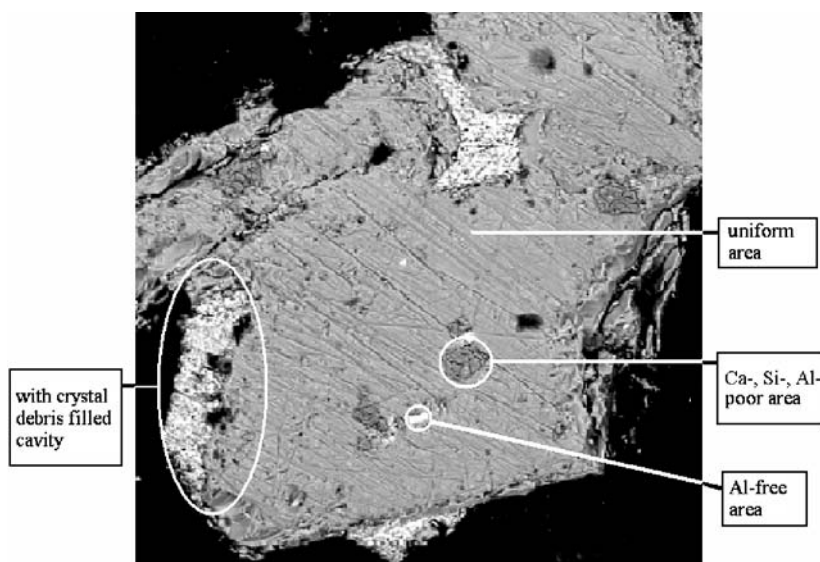**Fig. 5** Electron microscope picture using back-scattered electrons of single crystals of $Ca_5Si_2Al_2N_8$ embedded in methacrylate resin

the same direction. EDX analyses also show the exclusive presence of Ca, Si, Al and N/O. Furthermore, we have no evidence for the presence of carbon as all displacement parameters are in the typical range for nitridosilicates or nitridoaluminates. Hydrogen can be excluded as a result of the reaction conditions as niobium or tantalum gets transparent to hydrogen at temperatures above 600°C [32].

$Ca_4SiAl_3N_7$ is closely related to $Ca_5Si_2Al_2N_8$ and was therefore also investigated with the LA-ICP-MS method as there are no standards known for the Ca/Si/Al/N system. The results of the LA-ICP-MS analyses are summarised in Table 4.

Five replicate single-spot analyses were carried out on the same single crystal. Quantification was based on NIST 610 and internal standardisation using Ca (^{42}Ca using the nominal concentration of 43.63 wt% in $Ca_4SiAl_3N_7$). The isotopes ^{7}Li, ^{11}B, ^{23}Na, ^{25}Mg, ^{27}Al, ^{28,29,30}Si, ^{35}Cl, ^{39}K, $^{42-44}$Ca, ^{53}Cr, ^{55}Mn, ^{54,56,57}Fe, ^{72}Ge, ^{88}Sr, ^{90}Zr, ^{93}Nb, ^{153}Eu, ^{178}Hf and ^{181}Ta with limits of detection in the order of 1–10 ng g^{-1} were measured. Only the elements given in the table were significantly above the limits of detection. The ubiquitous occurrence of sodium was detected at an average concentration of 9 μg g^{-1}. Li, Cl, Fe, Sr, Zr, Eu and Ta and Eu are trace elements present in the single crystal with a maximum concentration of 100 μg g^{-1} (1–102 μg g^{-1}).

This crystal had a niobium concentration of 1.3 wt%, which can be interpreted by an inclusion of niobium in the single crystal, since the synthesis was performed in a closed niobium ampoule. We have no crystallographic evidence that Nb^{3+} is included in the crystal structure of $Ca_4SiAl_3N_7$ based on a detailed analysis of the structural data. Looking at the time-dependent ablation signal of ^{93}Nb, there is a maximum of the signal at the beginning and at the end of the measurement, pointing to metallic niobium located at the surface of the crystal. Another spike in the signal points to a metallic inclusion in the crystal. The

Fig. 6 Threefold zoom of the framed area from Fig. 5. *Captions* highlight the different areas in the single crystal

Table 9 Elemental analysis of the homogeneous grey area shown in Fig. 6 using EPMA

	Ca	Al	Si	Σ Al+Si	Absolute difference
Spot 1	44.80	13.17	10.46	23.63	2.43
Spot 2	44.79	12.88	10.63	23.51	2.55
Spot 3	45.24	13.48	10.18	23.66	2.40
Spot 4	45.49	13.44	10.67	24.11	1.95
Spot 5	43.77	12.83	10.50	23.33	2.73
Spot 6	45.73	13.60	10.57	24.17	1.89
Average	44.97	13.23	10.50	23.74	2.32
Norm	47.42	13.95	11.07	25.02	1.04
Standard deviation	0.73	0.34	0.19	0.53	0.53

All concentrations in wt%. Denoted are the concentrations for Ca, Al and Si, their sum and the absolute difference to the expected value of 26.06 wt%

Fig. 7 Electron microscope picture using back-scattered electrons of single crystals of $Ca_5Si_2Al_2N_8$ embedded in methacrylate resin. Areas investigated by scanning (*3, 4, 7–9*) or single-spot (*b3–b8*) LA-ICP-MS are marked with *white lines* or *circles*

corresponding signal increases by a factor of 50 in these areas.

However, the determined concentrations of Al and Si were determined to be significantly different from their theoretical concentration similar to $Ca_5Si_2Al_2N_8$. The sum of both elements was theoretically expected to be 29.68 wt% instead of the detected sum of 26.75 wt%. The absolute difference of 2.93 wt% from the expected value or the relative deviation of 9.9% was also not explainable by a contribution of another element present in the matrix. The individual concentration of Al at 22.21±0.91 wt% is very close to its expected concentration of 22.02 wt%. In contrast, the concentration of Si at 4.54±0.26 wt% was determined to be significantly below the theoretical value of 7.65 wt%.
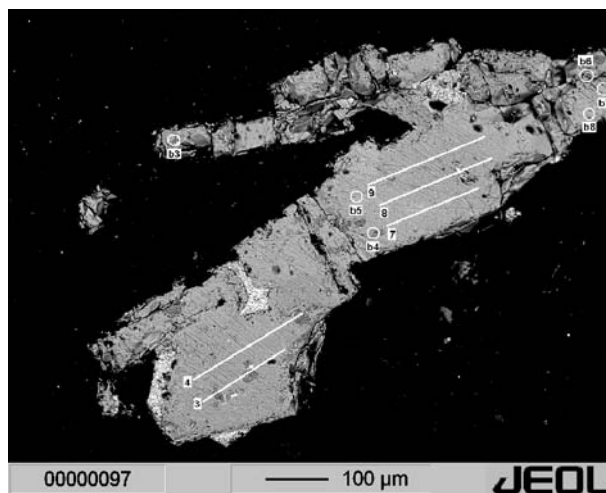
Moreover, the quantitative analysis of a second crystal of $Ca_4SiAl_3N_7$ leads to concentrations of Al and Si below expectations once again. The concentration for Al and Si are at 20.08±1.99 wt% and 4.50±0.31 wt%, respectively. The absolute discrepancy between expected and measured concentration is at 5.10 wt% with aluminium having a very high standard deviation pointing to a less homogeneous distribution of aluminium throughout the crystal.

Identical investigations were also performed on single crystals of $Ca_7Si_4N_{10}$ as there is no standard known for the Ca/Si/N system. All determined concentrations were standardized on ^{42}Ca using the nominal concentration of 52.64 wt% in $Ca_7Si_4N_{10}$. The concentrations of the LA-ICP-MS analyses on a $Ca_7Si_4N_{10}$ single crystal are summarised in Table 7.

The isotopes ^7Li, ^{11}B, ^{23}Na, ^{25}Mg, ^{27}Al, $^{29,30}Si$, $^{35,37}Cl$, ^{39}K, $^{42-44}Ca$, ^{57}Fe, ^{88}Sr, ^{93}Nb und ^{153}Eu with limits of detection in the order of 1–10 ng g^{-1} were measured. Only the elements given in the table were significantly above the limits of detection. The ubiquitous occurrence of sodium was not detected in this single crystal. Li, Mg, Cl, Fe, Sr and Nb are trace elements present in the single crystal with a maximum fraction of 237 ppm (1–237 µg g^{-1}). Surprisingly, this single crystal contains 2.63 wt% of aluminium pointing to a composition of $Ca_7Si_{4-x}Al_xN_{10-x}O_x$ with x≅0.5.

Nevertheless, the concentrations for Al and Si of 17.38 wt% were determined to be significantly different from their expected theoretical concentration. The sum concentration of both elements was expected to be 21.06 wt% instead of the detected 17.38 wt%. The absolute difference of 3.68 wt% from the expected value or the relative deviation of 21.1% was also not explainable by a contribution of other elements present in the matrix. The silicon concentration of 14.75±1.08 wt% points to significant differences in concentration throughout the crystal due to its high standard deviation.

The sum of the Al and Si concentrations in the first analysed $Ca_5Si_2Al_2N_8$ single crystal was the largest (23.43 wt%) measured out of twelve different single crystals of $Ca_5Si_2Al_2N_8$. The compositions and crystallographic properties of all these single crystals were thoroughly investigated by X-ray diffraction before subsequent single-spot LA-ICP-MS analyses. Table 8 summarises the Al and Si concentrations determined within these twelve crystals using two different external standards (NIST 610 and BCR2G). Both external reference materials (different in

Table 10 Elemental analysis of the bright (spots 7 and 8) and dark areas (spots 9–11) shown in Fig. 6 using EPMA

	Ca	Al	Si
Spot 7	52.32	0.09	35.74
Spot 8	52.52	0.11	34.03
Spot 9	37.92	5.84	6.12
Spot 10	38.54	6.29	5.88
Spot 11	42.68	7.19	5.89

Concentrations for Ca, Al and Si are in wt%

Table 11 Results of the scanning mode LA-ICP-MS analysis of $Ca_5Si_2Al_2N_8$ measured along the lines 3, 4, 7–9

	^7Li	^{11}B	^{25}Mg	^{27}Al	^{29}Si	^{30}Si	^{42}Ca	^{43}Ca	^{44}Ca	^{57}Fe	^{88}Sr	^{93}Nb
Replicate "3"	0	1	32	134,300	113,300	105,400	474,200	477,900	471,500	484	48	269
Replicate "4"	5	1	90	137,600	114,800	107,200	474,200	475,200	471,700	499	51	223
Replicate "7"	1	1	39	139,800	116,500	111,300	474,200	475,500	469,800	471	47	135
Replicate "8"	0	2	33	147,200	99,900	97,700	474,200	474,000	466,700	451	51	202
Replicate "9"	1	1	18	143,200	117,300	111,800	474,200	474,300	475,600	444	46	154
Average	1	1	42	140,420	112,360	106,680	474,200	475,380	471,060	470	49	197
Standard deviation	2	0	28	5,000	7,100	5,700		1,500	3,200	23	3	54

Ca was used as an internal standard, NIST 610 as an external standard, all concentrations in $\mu g\ g^{-1}$. The concentrations represent average concentrations of the analysed area

their absorptivity) were used to exclude matrix effects within the ICP. The concentrations determined using both reference materials are insignificantly different.

The average concentrations were 11.97±0.72 wt% for Al and 10.31±0.42 wt% for Si. The overall deviation of the determined concentration and the theoretical sum concentration Al+Si is at 3.78 wt%. Considering a total standard deviation of 1.14 wt%, the difference to the theoretical concentration remains significant. Furthermore, the multi-element analysis results indicate that no other major element was implemented into the crystal during synthesis.

Based on the concentration determination of Si and Al within $Ca_7Si_4N_{10}$, $Ca_4SiAl_3N_7$ and $Ca_5Si_2Al_2N_8$ and the results obtained on natural minerals it was necessary to use another analytical technique for cross validation of the results. Due to the fact the major element concentration differs by few wt%, EPMA at higher spatial resolution (10 instead of 60 μm), element-specific calibration and high suitability for major elements were applied to the same samples to get further insight into the Si/Al concentration ratios.

Therefore, single crystals of $Ca_5Si_2Al_2N_8$ were embedded in a methacrylate resin, the surface was polished and coated with a 20-nm layer of carbon. A thorough examination of the polished single crystals reveals red inclusions in the otherwise yellow crystals. One of these crystals and some of its splinters are shown in Fig. 4. The pictures were taken using an electron microscope with secondary electrons. The crystalline material appears light grey, the methacrylate resin dark grey. The surface rough-

ness of some micrometers has no influence for the determination of the composition.

Figure 5 shows the same area as in Fig. 4 but using back-scattered electrons. Different compositions result in different shades between light and dark grey. The outlined area in Fig. 5 shows several regions of different density and was therefore magnified three times as displayed in Fig. 6.

Three different, analytically relevant regions were identified (see Fig. 6): a homogeneous medium grey region, an aluminium-free light grey region and a dark grey Ca-, Si- and Al-poor region. Marginal cavities filled with crystal debris were not investigated and appear in a very light grey. Table 9 shows the results of the elemental analysis of the homogeneous grey area shown in Fig. 6 using EPMA. As there are no internal but external standards only for this investigation, the detected value for calcium was normalised to the nominal concentration of 47.42 wt% (cf. line "norm").

The EPMA analyses shows that the aluminium value is 2.0 wt% higher than the average concentration determined by LA-ICP-MS (Table 8), whereas the silicon concentration increases by 0.8 wt%. That results in a sum concentration of Al+Si of 25.02±0.53 wt%, which is significantly higher in comparison to the 22.28 wt% determined by LA-ICP-MS (Table 8). The concentrations of aluminium, calcium and silicon are reproducible throughout the entire homogeneous area of the crystal. This value is in good agreement with the theoretical sum concentration of 26.06 wt% when considering the standard deviation of 0.53 wt%. Based on the analysis of the homogeneous area one

Table 12 Results of the 30-μm single-spot LA-ICP-MS analyses of the embedded $Ca_5Si_2Al_2N_8$ single crystal using calcium as an internal standard, NIST 610 as an external standard; all concentrations in $\mu g\ g^{-1}$

Isotope	^7Li	^{11}B	^{25}Mg	^{27}Al	^{29}Si	^{30}Si	^{42}Ca	^{43}Ca	^{44}Ca	^{57}Fe	^{88}Sr	^{93}Nb
Replicate "b3"	0	1	12	128,300	109,500	104,400	474,200	481,500	476,800	432	52	254
Replicate "b4"	0	1	8	131,900	109,000	107,300	474,200	530,500	480,400	460	47	282
Replicate "b5"	0	1	2	131,000	106,100	108,400	474,200	475,700	477,900	424	43	139
Replicate "b6"	0	1	11	127,000	108,400	102,500	474,200	463,500	462,800	455	56	130
Replicate "b7"	0	1	6	133,200	106,000	106,000	474,200	475,000	476,000	448	66	223
Replicate "b8"	1	2	8	123,600	113,200	106,700	474,200	485,200	472,700	428	89	99
Average	0	1	8	129,167	108,700	108,700	474,200	485,233	474,433	441	59	188
Standard deviation	0	0	3	3,600	2,700	2,100		23,400	6,200	5	17	75

can derive an empirical formula of $Ca_5Si_{1.7}Al_{2.2}O_xN_{8-x}$ ($x\cong0.25$) where values for oxygen and nitrogen were estimated based on the electroneutrality. Two other single crystals of this material were analysed in a similar manner revealing the following compositions: $Ca_5Si_{1.7}Al_{2.2}O_xN_{8-x}$ ($x\cong0.25$) and $Ca_5Si_{1.5}Al_{2.4}O_xN_{8-x}$ ($x\cong0.45$).

However, the EPMA analysis of the other light (spots 7+8) and dark grey areas (spots 9–11) lead to concentrations, which indicate different phase composition within the same single crystal. Table 10 summarises the results of these areas.

The light grey areas are nearly free of aluminium with a Ca:Si mass ratio of 1.5:1, whereas the dark grey areas contain less aluminium, silicon and calcium compared to the homogeneous region. These dark areas appear red and transparent when examined through an optical microscope and cannot be assigned to any known nitridoaluminosilicate. Silicides and aluminidesilicides can be excluded due to the transparent appearance of the entire material and the missing difference to 100 wt%. Therefore, we can only conclude that these regions could consist of unknown crystalline silicates or amorphous, vitreous materials. However, the exact determination has been unsuccessful so far.

For a verification of the results of the EPMA analysis, LA-ICP-MS was used in scanning mode, in which the laser samples a larger area across the crystal. The purpose of this study was to explain the different concentrations determined by single-spot LA-ICP-MS and EPMA analysis. Scanning mode LA-ICP-MS allows a continuous monitoring of the elemental composition of different sample areas. The sample is therefore moved during the laser sampling process. A similar type of 193 nm ArF excimer laser (Geolas Q, MicroLas Göttingen) with a spatial resolution of 30 μm was used for sample ablation. The well-characterized sample (Fig. 7) was used again for the scanning laser analyses. The 20-nm carbon coating on the surface was removed to prevent the formation of $^{12}C^{16}O$ and a subsequent interference on ^{28}Si. The scanning mode was performed along the lines (3–9) shown in Fig. 7. Furthermore, a comparison with the single-spot method using a 30-μm-diameter laser was also carried out (b3–b8). The results of the scanning mode LA-ICP-MS are summarised in Table 11.

The sum concentration of Al+Si for the scanned areas led to an average concentration of 25.28±1.31 wt%, which is in good agreement with the theoretical and expected concentration of 26.06 wt%. The lower concentrations for ^{27}Al in scan "3" and "4" are possibly caused by Al-free regions as demonstrated by EPMA. These results show that the resultant concentrations describe the sample in a more lifelike way than the single-spot method.

An additional investigation of the abovementioned crystal with a 30-μm single-spot LA-ICP-MS leads not surprisingly to sum concentrations of Al and Si which are too low due to the detected inhomogeneities in the crystal. Table 12 gives the results of this investigation.

Conclusions

The chemical composition of single crystals investigated by X-ray was analyzed quantitatively using single-spot LA-ICP-MS. The cooperative use of a microprobe and a raster LA-ICP-MS leads to the discovery of inclusions in single crystals of $Ca_5Si_2Al_2N_8$. These impurities were not detected by standard X-ray examination methods. It is likely that these impurities consist of either cocrystallised oxo- or nitridosilicates or amorphous, vitreous phases. X-ray powder diffraction data indicates the existence of a significant fraction of an X-ray amorphous material besides crystalline silicates. The application of a standard single-spot LA-ICP-MS with a spatial resolution of 60 or 30 μm is not suitable for the analysis of these crystals as the existing inhomogeneities dominate and alter the determined concentrations. This single-spot method always yields concentrations for the sum of Al and Si for these crystals which are too low in comparison to the theoretical values. High spatial resolution analysis using EPMA (10 μm) leads to the discovery of inhomogeneities in the crystalline material. However, owing to the better detection capabilities, a scanning LA-ICP-MS procedure enables a more representative analysis of single crystals of $Ca_5Si_2Al_2N_8$ than single-spot LA-ICP-MS as a result of a larger sampling volume.

The excellent R factors of the single crystals derived from X-ray analysis of between 1.5 and 3.0 give no indication for these differences in composition. Therefore, we assume that these crystals are intergrown with unknown crystalline, amorphous or vitreous phases related to oxo- or nitridosilicates.

References

1. Lissner F, Schleid T (2004) Z Anorg Allg Chem 630:2226–2230
2. Gál ZA, Mallinson PM, Orchard HJ, Clarke SJ (2004) Inorg Chem 43:3998–4006
3. Orth M, Schnick W (1999) Z Anorg Allg Chem 625:1426–1428
4. Huppertz H, Schnick W (1998) Z Anorg Allg Chem 624:371–374
5. Huppertz H, Schnick W (1997) Z Anorg Allg Chem 623:212–217
6. Huppertz H, Schnick W (1997) Angew Chem 109:2765–2767; Angew Chem Int Ed Engl 36:2651–2652
7. Huppertz H, Schnick W (1997) Acta Crystallogr Sect C53: 1751–1753
8. Huppertz H, Schnick W (1997) Chem Eur J 3:249–252
9. Huppertz H, Schnick W (1997) Chem Eur J 3:679–683 (For an overview of publications on nitridosilicates published before 1997)
10. Durrant SF (1999) J Anal At Spectrom 14:1385–1404
11. Günther D, Jackson SE, Longerich HP (1999) Spectrochim Acta B54:381–409

12. Becker JS, Pickhardt C, Dietze HJ (2000) Mikrochim Acta 135:71–80
13. Heinrich CA, Pettke T, Halter WE, Aigner-Torres M, Audetat A, Günther D, Hattendorf B, Bleiner D, Guillong M, Horn I (2003) Geochim Cosmochim Acta 67:3473–3497
14. Sinclair DJ, Kinsley LPJ, Mcculloch MT (1998) Geochim Cosmochim Acta 62:1889–1901
15. Baker SA, Bi M, Aucelio RQ, Smith BW, Winefordner JD (1999) J Anal At Spectrom 14:19–26
16. Koch J, Feldmann I, Hattendorf B, Günther D, Engel U, Jakubowski N, Bolshov M, Niemax K, Hergenroder R (2002) Spectrochim Acta B57:1057–1070
17. Pickhardt C, Brenner IB, Becker JS, Dietze HJ (2000) Fresenius J Anal Chem 368:79–87
18. Haberecht J, Hametner K, Nesper R, Günther D (2005) Chem Mat (in press)
19. Russo RE, Mao XL, Liu HC, Gonzalez J, Mao SS (2002) Talanta 57:425–451
20. Ottinger F (2004) Dissertation No. 15624, ETH Zurich, Switzerland
21. Longerich HP, Jackson SE, Günther D (1996) J Anal At Spectrom 11:899–904
22. Jackson SE, Longerich HP, Dunning GR, Freyer BJ (1992) Can Mineral 30:1049–1064
23. Fryer BJ, Jackson SE, Longerich HP (1995) Can Mineral 33:303–312
24. Longerich HP, Günther D, Jackson SE (1996) Fresenius J Anal Chem 355:538–542
25. Kuhn HR, Guillong M, Günther D (2004) Anal Bioanal Chem 378:1069–1074
26. Guillong M, Kuhn HR, Günther D (2003) Spectrochim Acta B58:211–220
27. Armstrong JT (1993) In: Proceedings of the 27th Annual MAS Meeting. Caltech, pp S13–14
28. Jeffries TE, Jackson SE, Longerich HP (1998) J Anal At Spectrom 13:935–941
29. Jeffries TE, Perkins WT, Pearce NJG (1995) Analyst 120: 1365–1372
30. Guillong M, Horn I, Günther D (2003) J Anal At Spectrom 18:1224–1230
31. Kuhn HR, Günther D (2004) J Anal At Spectrom 19:1158–1164
32. Leon-Escamilla EA, Corbett JD (1998) J Alloys Compd 265: 104–114